



A symbolic framework for flexible multibody systems applied to horizontal axis wind turbines

Emmanuel Branlard¹ and Jens Geisler²

¹National Renewable Energy Laboratory, Golden, CO 80401, USA

²Hochschule Flensburg, University of Applied Sciences, 24943 Flensburg, Germany

Correspondence: E. Branlard (emmanuel.branlard@nrel.gov)

1 **Abstract.** The article presents a symbolic framework that is used to obtain the linear and non-linear equations of motion
2 of a multibody system including rigid and flexible bodies. Our approach is based on Kane's method and a nonlinear shape
3 function representation for flexible bodies. The method yields compact symbolic equations of motion with implicit account of
4 the constraints. The general and automatic framework facilitate the creation and manipulation of models with various levels
5 of fidelity. The symbolic treatment allows for the obtention of analytical gradients and linearized equations of motion. The
6 linear and non-linear equations can be exported to Python code or dedicated software. The application are multiple such as:
7 time-domain simulation, stability analyses, frequency domain analyses, advanced controller design, state observers, digital
8 twins, etc. In this paper, we describe the method we used to systematically generate the equations of motion of multibody
9 systems. We apply the framework to generate illustrative onshore and offshore wind turbine models. We compare our results
10 with OpenFAST simulations and discuss the advantages and limitations of the method. A Python implementation is provided
11 as an opensource project.

12 1 Introduction

13 The next generation of wind turbine digital technologies requires versatile aero-servo-hydro-elastic models, with various levels
14 of fidelity, suitable for a wide range of applications. Such applications include: time domain simulations, linearization (for
15 controller design and tuning, or frequency domain analyses), analytical gradients (for optimization procedures), generation of
16 dedicated, high-performance or embedded code (for standalone simulations, state observers or digital twins). Current mod-
17 els are implemented for a specific purpose and usually based on an heuristic structure. Aeroelastic tools, such as Flex (Øye,
18 1983; Branlard, 2019) or ElastoDyn (OpenFAST, 2021), rely on: an assumed chain of connections between bodies, a given
19 set of degrees of freedom, and predefined orientations of shape functions. Tools with linearization capabilities, such as hawc-
20 stab2 (Sønderby and Hansen, 2014) or OpenFAST (OpenFAST, 2021) are dedicated to horizontal axis wind turbines and the
21 evaluation of the gradients are limited to hard-coded analytical expressions or numerical finite-differences. Small implemen-
22 tation changes often require an extensive redevelopment, and the range of applications of the tools remain limited (Simani,
23 2015).



24 To address this issue, we propose a framework for the automatic derivation, processing and parametrization of models with
25 granularity in the level of fidelity. Our approach is based on Kane’s method (Kane and Wang, 1965) and a nonlinear shape
26 function representation of flexible bodies (Shabana, 2013) described using a standard input data (SID) format (Wallrapp, 1994;
27 Schwertassek and Wallrapp, 1999). The method yields compact symbolic equations of motion with implicit account of the
28 constraints. Similar approaches have been presented in the literature: Kurz and Eberhard (2009), Merz (2018), Lemmer (2018),
29 Branlard (2019). Our framework differs in the fact that all equations are processed at a symbolic level and therefore the model
30 can be used in its nonlinear or linearized form. We implemented an open-source version in Python using SymPy (SymPy),
31 leveraging its mechanical toolbox. Alternative symbolic frameworks found in the literature are usually limited to rigid bodies
32 (Verlinden et al., 2005; Kurz and Eberhard, 2009; Gede et al., 2013; Docquier et al., 2013), or closed-source (Reckdahl and
33 Mitiguy, 1996; Kurtz et al., 2010; MotionGenesis, 2016), and cannot be directly processed in Python.

34 In section 2, we present the formalism used to derive the equations of motion. In section 3, we given an overview of how the
35 equations were implemented into a symbolic calculation framework, to easily manipulate the equations and generate dedicated
36 code. Example of applications relevant to wind energy are given in section 4. Discussions and conclusions follow.

37 2 Method to obtain the equations of motion

38 In this section, we present the formalism used to setup the equations of motion.

39 2.1 System definition and kinematics

40 We consider a system of n_b bodies, rigid or flexible, connected by a set of joints. For simplicity, we assume that no kinematic
41 loops are present in the system, and the mass of the bodies are constant. An inertial frame is defined to express the positions,
42 velocities and accelerations of the bodies. We adopt a minimal set of generalized coordinates, \mathbf{q} , of dimension n_q , to describe
43 the kinematics of the bodies: joint coordinates describing the joints displacements, and Rayleigh-Ritz coordinates for the
44 amplitudes of the shape functions of the flexible bodies (see, e.g. Branlard (2019)). The choice of coordinates is left to the user,
45 but it is assumed to form a minimal set. We will provide illustrative examples in section 4.

46 At a given time, the positions, orientations, velocities, and accelerations of all the points of the structure are entirely deter-
47 mined by the knowledge of \mathbf{q} , $\dot{\mathbf{q}}$ and $\ddot{\mathbf{q}}$. For a given body i , and a point P belonging to the body, the position, velocity and
48 acceleration of the point are given by (see e.g. Shabana (2013)):

$$49 \mathbf{r}_P = \mathbf{r}_i + \mathbf{s}_P = \mathbf{r}_i + \mathbf{s}_{P_0} + \mathbf{u}_P \quad (1)$$

$$50 \mathbf{v}_P = \mathbf{v}_i + \boldsymbol{\omega}_i \times \mathbf{s}_P + (\dot{\mathbf{u}}_P)_i \quad (2)$$

$$51 \mathbf{a}_P = \mathbf{a}_i + \boldsymbol{\omega}_i \times (\boldsymbol{\omega}_i \times \mathbf{s}_P) + \dot{\boldsymbol{\omega}}_i \times \mathbf{s}_P + 2\boldsymbol{\omega}_i \times (\dot{\mathbf{u}}_P)_i + (\ddot{\mathbf{u}}_P)_i \quad (3)$$

52 where: \mathbf{r}_i , \mathbf{v}_i and \mathbf{a}_i are the position, velocity and acceleration of the origin of the body; \mathbf{s}_{P_0} is the initial (undeformed)
53 position vector of point P with respect to the body origin; \mathbf{u}_P is the elastic displacement of the point (0 for rigid bodies);
54 $\boldsymbol{\omega}_i$ is the rotational velocity of the body with respect to the inertial frame; (\cdot) and $(\cdot)_i$ refer to time derivatives in the inertial



55 and body frame respectively. Throughout the paper, we use bold symbols for vectors and matrices, and uppercase symbols
 56 for most matrices. The elastic displacement is obtained as a superposition of elastic deformations (see subsection 2.4). We
 57 define the transformation matrix \mathbf{R}_i which transforms coordinates from the body frame to the inertial frame, and by definition
 58 $[\tilde{\omega}_i] = \dot{\mathbf{R}}_i \mathbf{R}_i^T$, where $[\tilde{\cdot}]$ represents the skew symmetric matrix.

59 2.2 Introduction to Kane's method

60 Kane's method (Kane and Wang, 1965) is a powerful and systematic way to obtain the equations of motion of a system. The
 61 procedure leads to n_q coupled equations of motion:

$$62 \quad \mathbf{f}_r + \mathbf{f}_r^* = 0, \quad r = 1 \dots n_q \quad (4)$$

63 where \mathbf{f}_r^* is associated with inertial loads and \mathbf{f}_r is associated with external loads, and these components are obtained for each
 64 generalized coordinates. The components are obtained as a superposition of contributions from each body:

$$65 \quad \mathbf{f}_r = \sum_{i=1}^{n_b} \mathbf{f}_{ri}, \quad \mathbf{f}_r^* = \sum_{i=1}^{n_b} \mathbf{f}_{ri}^* \quad (5)$$

66 The terms \mathbf{f}_{ri} and \mathbf{f}_{ri}^* can be obtained for each body individually and assembled at the end to form the final system of equa-
 67 tions. We will present in subsection 2.3 and subsection 2.4 how these terms are defined for rigid bodies and flexible bodies
 68 respectively.

69 2.3 Rigid bodies

70 We assume that body i is a rigid body and proceed to define the terms \mathbf{f}_{ri} and \mathbf{f}_{ri}^* . The inertial force, \mathbf{f}_i^* , and inertial torque,
 71 $\boldsymbol{\tau}_i^*$, acting on the body are:

$$72 \quad \mathbf{f}_i^* = -m_i \mathbf{a}_{G,i}, \quad \boldsymbol{\tau}_i^* = -\mathbf{I}_{G,i} \cdot \dot{\boldsymbol{\omega}}_i - \boldsymbol{\omega}_i \times (\mathbf{I}_{G,i} \cdot \boldsymbol{\omega}_i) \quad (6)$$

73 where m_i is the mass of the body, $\mathbf{a}_{G,i}$ is the acceleration of its center of mass with respect to the inertial frame, $\mathbf{I}_{G,i}$ is the
 74 inertial tensor of the body expressed at its center of mass. Equation 6 is a vectorial relationship, it may therefore be evaluated
 75 in any coordinate system. The component f_{ri}^* is defined as:

$$76 \quad \mathbf{f}_{ri}^* = \mathbf{J}_{v,ri} \cdot \mathbf{f}_i^* + \mathbf{J}_{\omega,ri} \cdot \boldsymbol{\tau}_i^* \quad (7)$$

77 with

$$78 \quad \mathbf{J}_{v,ri} = \frac{\partial \mathbf{v}_{G,i}}{\partial \dot{q}_r}, \quad \mathbf{J}_{\omega,ri} = \frac{\partial \boldsymbol{\omega}_i}{\partial \dot{q}_r} \quad (8)$$

79 where $\mathbf{v}_{G,i}$ is the velocity of the body masscenter with respect to the inertial frame. The partial velocities, or Jacobians, \mathbf{J}_v
 80 and \mathbf{J}_ω , are key variables of the Kane's method. They project the physical coordinates into the generalized coordinates (\mathbf{q}),
 81 inherently accounting for the kinematic constraints between bodies. In numerical implementations, the Jacobians are typically



82 stored in matricial forms, referred to as velocity transformation matrices. The terms f_{ri}^* can equivalently be obtained using the
 83 partial velocity of any body point (e.g. the origin) by carefully transferring the inertial loads to the chosen point. The external
 84 forces and torques acting on the body are combined into an equivalent force and torque acting at the center of mass, written f_i
 85 and τ_i . The component f_{ri} is then given by:

$$86 \quad f_{ri} = J_{v,ri} \cdot f_i + J_{\omega,ri} \cdot \tau_i \quad (9)$$

87 Equivalently, the contributions from each individual force, $f_{i,j}$, acting on a point P_j of the body i , and each individual torques,
 88 $\tau_{i,k}$, can be summed using the appropriate partial velocity to obtain f_{ri} :

$$89 \quad f_{ri} = \sum_j \frac{\partial v_{P_j}}{\partial \dot{q}_r} \cdot f_{i,j} + \sum_k J_{\omega,ri} \cdot \tau_{i,k} \quad (10)$$

90 where v_{P_j} is the velocity of the point j with respect to the inertial frame. Equation 7 and Equation 9 are inserted in Equation 5
 91 to obtain the final equations of motion.

92 2.4 Flexible bodies

93 We assume that body i is a flexible body and proceed to define the terms f_{ri} and f_{ri}^* . The dynamics of a flexible body is described
 94 in standards textbooks such as Shabana (2013) or Schwertassek and Wallrapp (1999). Unlike rigid bodies, the equations for
 95 flexible bodies are typically expressed with respect to a reference point different from the center of mass. We will call this point
 96 the origin and write it O_i . The elastic displacement field of the body is written u . It defines the displacement of any point of
 97 the body with respect to its undeformed position. Using the first order¹ Rayleigh-Ritz approximation, the displacement field at
 98 a given point, P , is given by the sum of shape function contributions: $u(P) = \sum_{j=1}^{n_{e,i}} \Phi_{ij}(P) q_{e,ij}(t)$, where Φ_{ij} are the shape
 99 functions (displacement fields) of body i and $q_{e,ij}$ is the subset of q consisting of the elastic coordinates of body i , of size $n_{e,i}$.
 100 The principles of the shape function approach applied to beams are given in Appendix B. The shape functions are more easily
 101 represented in the body coordinate system. Vectors and matrices that are explicitly written in the body frame will be written
 102 with primes. The equations of motion of the flexible bodies are (Wallrapp, 1994):

$$103 \quad \begin{bmatrix} M'_{xx} & M'_{x\theta} & M'_{xe} \\ & M'_{\theta\theta} & M'_{\theta e} \\ \text{sym.} & & M'_{ee} \end{bmatrix}_i \begin{bmatrix} a'_i \\ \dot{\omega}_i \\ \ddot{q}_{e,i} \end{bmatrix} + \begin{bmatrix} k'_{\omega,x} \\ k'_{\omega,\theta} \\ k'_{\omega,e} \end{bmatrix}_i + \begin{bmatrix} 0 \\ 0 \\ k_e \end{bmatrix}_i = \begin{bmatrix} f'_x \\ f'_\theta \\ f'_e \end{bmatrix}_i \quad (11)$$

104 with: x, θ, e , subscripts that indicate the translation, rotation and elastic components; M , the mass matrix of dimension $6 + n_{e,i}$
 105 made of the block matrices M_{xx}, \dots, M_{ee} ; a_i and $\dot{\omega}_i$, the linear and angular acceleration of the body (origin) with respect to
 106 the inertial frame; k_ω , the centrifugal, gyration and Coriolis loads, also called quadratic velocities loads; k_e , the elastic strain
 107 loads; f , the external forces, torques and elastic generalized forces. The different components of M , k_ω , k_e and f are given

¹We address the second order approximation in subsection 5.3 and Appendix C.



108 in Appendix A. These terms depend on \mathbf{q} , $\dot{\mathbf{q}}$, and Φ_i . The inertial force, torque and elastic loads are:

$$109 \quad \mathbf{f}_i^* = -\mathbf{R}_i \left[\mathbf{M}'_{xx} \mathbf{a}'_i + \mathbf{M}'_{x\theta} \dot{\boldsymbol{\omega}}'_i + \mathbf{M}'_{xe} \ddot{\mathbf{q}}_{e,i} + \mathbf{k}'_{\omega,x} \right] \quad (12)$$

$$110 \quad \boldsymbol{\tau}_i^* = -\mathbf{R}_i \left[\mathbf{M}'_{\theta x} \mathbf{a}'_i + \mathbf{M}'_{\theta\theta} \dot{\boldsymbol{\omega}}'_i + \mathbf{M}'_{\theta e} \ddot{\mathbf{q}}_{e,i} + \mathbf{k}'_{\omega,\theta} \right] \quad (13)$$

$$111 \quad \mathbf{h}_i^* = - \left[\mathbf{M}'_{ex} \mathbf{a}'_i + \mathbf{M}'_{e\theta} \dot{\boldsymbol{\omega}}'_i + \mathbf{M}'_{ee} \ddot{\mathbf{q}}_{e,i} + \mathbf{k}'_{\omega,e} \right] \quad (14)$$

112 The external and elastic loads are:

$$113 \quad \mathbf{f}_i = \mathbf{R}_i \mathbf{f}'_x \quad (15)$$

$$114 \quad \boldsymbol{\tau}_i = \mathbf{R}_i \mathbf{f}'_\theta \quad (16)$$

$$115 \quad \mathbf{h}_i = \mathbf{f}_e - \mathbf{k}_e \quad (17)$$

116 The component of \mathbf{f}_{ri}^* and \mathbf{f}_{ri} , for $r = 1 \dots n_q$, are then defined as:

$$117 \quad \mathbf{f}_{ri}^* = \mathbf{J}_{v,ri} \cdot \mathbf{f}_i^* + \mathbf{J}_{\omega,ri} \cdot \boldsymbol{\tau}_i^* + \mathbf{J}_{e,ri} \cdot \mathbf{h}_i^* \quad (18)$$

$$118 \quad \mathbf{f}_{ri} = \mathbf{J}_{v,ri} \cdot \mathbf{f}_i + \mathbf{J}_{\omega,ri} \cdot \boldsymbol{\tau}_i + \mathbf{J}_{e,ri} \cdot \mathbf{h}_i \quad (19)$$

119 with

$$120 \quad \mathbf{J}_{v,ri} = \frac{\partial \mathbf{v}_{O,i}}{\partial \dot{q}_r}, \quad \mathbf{J}_{\omega,ri} = \frac{\partial \boldsymbol{\omega}_i}{\partial \dot{q}_r}, \quad \mathbf{J}_{e,ri} = \frac{\partial \mathbf{q}_{e,i}}{\partial q_r} \quad (20)$$

121 where $\mathbf{v}_{O,i}$ is the velocity of the body with respect to the inertial frame. The term $\mathbf{J}_{e,ri}$ consists of 0 and 1 because $\mathbf{q}_{e,i}$ is a
 122 subset of \mathbf{q} . Equation 18 and Equation 19, once evaluated for body i , are inserted in Equation 5 to obtain the final equations of
 123 motion.

124 2.5 Non-linear and linear equations of motion

125 The n_q equations of motion given in Equation 4 are gathered into a vertical vector \mathbf{e} . They are recast into the form:

$$126 \quad \mathbf{e}(\mathbf{q}, \dot{\mathbf{q}}, \ddot{\mathbf{q}}, \mathbf{u}, t) = \mathbf{f} + \mathbf{f}^* = \mathbf{F}(\mathbf{q}, \dot{\mathbf{q}}, \mathbf{u}, t) - \mathbf{M}(\mathbf{q}) \ddot{\mathbf{q}} = \mathbf{0} \quad (21)$$

127 or

$$128 \quad \mathbf{M}(\mathbf{q}) \ddot{\mathbf{q}} = \mathbf{F}(\mathbf{q}, \dot{\mathbf{q}}, \mathbf{u}, t) \quad (22)$$

129 where $\mathbf{M} = -\frac{\partial \mathbf{e}}{\partial \ddot{\mathbf{q}}}$ is the system mass matrix, and \mathbf{F} is the forcing term vector, that is, the reminder terms of the equation
 130 ($\mathbf{F} = \mathbf{e} + \mathbf{M} \ddot{\mathbf{q}}$). The vector \mathbf{u} is introduced to represent the time dependent inputs that are involved in the determination of the
 131 external loads. Both sides of the equations are also dependent on some parameters but this dependency is omitted to shorten
 132 notations. The stiffness and damping matrices may be obtained by computing the Jacobian of the equations of motion with
 133 respect to \mathbf{q} and $\dot{\mathbf{q}}$ respectively. The non-linear equation given in Equation 22 is easily integrated numerically, for instance by
 134 recasting the system into a first order system, or by using dedicated second order system time integrator.



135 In various applications, a linear time invariant approximation of the system is desired. Such approximation is obtained at an
136 operating point, noted with the subscript 0, which is a solution of the non-linear equations of motion, viz:

$$137 \quad \mathbf{e}(\mathbf{q}_0, \dot{\mathbf{q}}_0, \ddot{\mathbf{q}}_0, \mathbf{u}_0, t) = \mathbf{0} \quad (23)$$

138 The linearized equations about this operating point are obtained using a Taylor-Series expansion:

$$139 \quad \mathbf{M}_0(\mathbf{q}_0) \delta \ddot{\mathbf{q}} + \mathbf{C}_0(\mathbf{q}_0, \dot{\mathbf{q}}_0, \mathbf{u}_0) \delta \dot{\mathbf{q}} + \mathbf{K}_0(\mathbf{q}_0, \dot{\mathbf{q}}_0, \mathbf{u}_0) \delta \mathbf{q} = \mathbf{Q}_0(\mathbf{q}_0, \dot{\mathbf{q}}_0, \mathbf{u}_0) \delta \mathbf{u} \quad (24)$$

140 with

$$141 \quad \mathbf{M}_0 = - \left. \frac{\partial \mathbf{e}}{\partial \ddot{\mathbf{q}}} \right|_0, \mathbf{C}_0 = - \left. \frac{\partial \mathbf{e}}{\partial \dot{\mathbf{q}}} \right|_0, \mathbf{K}_0 = - \left. \frac{\partial \mathbf{e}}{\partial \mathbf{q}} \right|_0, \mathbf{Q}_0 = \left. \frac{\partial \mathbf{e}}{\partial \mathbf{u}} \right|_0 \quad (25)$$

142 where \mathbf{M}_0 , \mathbf{C}_0 , \mathbf{K}_0 are the linear mass, damping, and stiffness matrices, \mathbf{Q}_0 is the linear forcing vector, δ indicate a small
143 perturbation of the quantities, and $|_0$ indicates that the expressions are evaluated at the operating point. Examples of application
144 of the linear equations of motion are: controller design, frequency domain analyses, stability analyses.

145 3 Implementation into a symbolic framework

146 In this section we discuss a Python open-source symbolic calculation framework that implements the equations given in sec-
147 tion 2. A Maxima implementation from the same authors is also available Geisler (2021).

148 The python library YAMS (Yet Another Multibody Solver) started as a numerical tool published in previous work (Branlard,
149 2019). The library is now supplemented with a symbolic module so that both numerical and symbolic calculations can be
150 achieved. The new implementation uses the python symbolic calculation package SymPy (SymPy). We leveraged the features
151 present in the subpackage “mechanics”, which contains all the tools necessary to compute kinematics: definition of frames
152 and points, and determination of positions, velocities, and accelerations. The subpackage also contains an implementation of
153 Kane’s equations for rigid body (i.e. subsection 2.3). We were also inspired by the package PyDy (Gede et al., 2013), which is
154 a convenient tool to export the equations of motion to executable code, and directly visualize the bodies in 3D. The core of our
155 work consisted in implementing a class to define flexible bodies (`FlexibleBody`) and the corresponding Kane’s method for
156 this class (subsection 2.4).

157 For the `FlexibleBody` class, we followed the formalism of Wallrapp (1994), and implemented Taylor expansions for all
158 the terms defined in Appendix A, allowing the symbolic computation with shape functions of any order. The different Taylor
159 coefficients may be kept as symbolic terms, or replaced early on by numerical values provided for instance by an SID.

160 We structured the code into three layers. 1) The low-level layer integrates seamlessly with SymPy and PyDy, by using
161 the `FlexibleBody` class we provide. It is the layer which offers the highest level of granularity and control for the user,
162 since arbitrary systems with various kinematic constraints can be implemented, at the cost of requiring more expertise. 2) The
163 second-level automates the calculation of the kinematics, by introducing simple connections between rigid and flexible bodies.
164 The connections may be rigid, with constant offsets and rotations, or dynamic. A connection from a flexible body to another



165 body is assumed to occur at one extremity of the flexible body. Some knowledge of SymPy mechanics are still required to use
166 this layer. 3) The third level consists of template models such as generic onshore or offshore wind turbine models. Degrees of
167 freedom are easily turned on and off for these models depending on the level of fidelity asked by the user and generic external
168 forces can be implemented or declared as external inputs. The non-linear and linear equations of motion can be exported to
169 latex and python-ready scripts for various applications (see subsection 5.1). As little as three lines of code are required by
170 the user to perform the full step from derivation of the equations, optional linearization, and exportation. To obtain numerical
171 results from the exported python code, the user needs to provide the arrays with the degrees of freedom values \mathbf{q} and $\dot{\mathbf{q}}$, their
172 initial conditions, a dictionary with inputs (\mathbf{u}) that are function of time, and a dictionary of parameters (\mathbf{p}) containing all the
173 numerical constants such as mass, acceleration of gravity, etc. We provide tools to readily time-integrate the generated model
174 using numerical values (including initial values) from a set of OpenFAST input files.

175 The source code of YAMS is available on github as a subpackage of the Wind Energy LIBrary, WELIB (Branlard, 2021).
176 The repository contains tests and working examples, including the ones presented in section 4. The finite element package of
177 the repository can be used to generate the SID from beam models such as the ones used for blades and tower.

178 4 Wind energy applications

179 4.1 Approach

180 In this section we present different wind energy applications of the symbolic framework. We focus on models with at least
181 one flexible body since the rigid-body formulation of SymPy has been well verified (Gede et al., 2013). For each example,
182 the equations of motion are given and their results are compared with OpenFAST (OpenFAST, 2021) simulations. This is
183 readily achieved because our framework can export the equations of motion to python functions, load input files from an
184 OpenFAST model, and integrate the generated equations using the same conditions as defined in the OpenFAST input files. In
185 this article, we do not focus on the modelling of the external loads but we include them in the equations of motion. It is the
186 responsibility of the user to define these functions, for instance through aero- or hydro-force models. For the verification results
187 presented in this section we only include the gravitational and inertial loading. In all examples, the NREL 5-MW reference
188 wind turbine (Jonkman et al., 2009) is used. The examples below are provided on the github repository where the YAMS
189 package is provided (Branlard, 2021).

190 4.2 Notations

191 We adopt a system of notations where the first letter of a body is used to identify the parameters of this body. As an example,
192 the tower is represented with the letter T, and the following body parameters are defined: T , origin; M_T , mass; L_T , length;
193 $(J_{x,T}, J_{y,T}, J_{z,T})$, diagonal coefficients of the inertia tensor about the center of gravity and in body-coordinates; \mathbf{r}_{TG} , vector
194 from body origin to body center of mass, of coordinates (x_{TG}, y_{TG}, z_{TG}) in body-coordinates. We also define: θ_t , the nacelle
195 tilt angle about the y axis; g the acceleration of gravity along $-z$; O the origin of the global coordinate system.



196 4.3 Rotating blade with centrifugal stiffening

197 We begin with the study of a flexible blade of length $L_B = R$, rotating at the constant rotational speed Ω . We use this test case
 198 to familiarize the reader with the key concepts of the shape function approach given in Appendix B. A sketch of the system
 199 is given in Figure 1. We start by modelling the blade using a single shape function, assumed to be directed along the x axis
 (“flapwise”): $\hat{\Phi}_1 = \hat{\Phi}\hat{x}$, where the hat notation indicates the unit vector in the x direction. The undeflected blade is directed

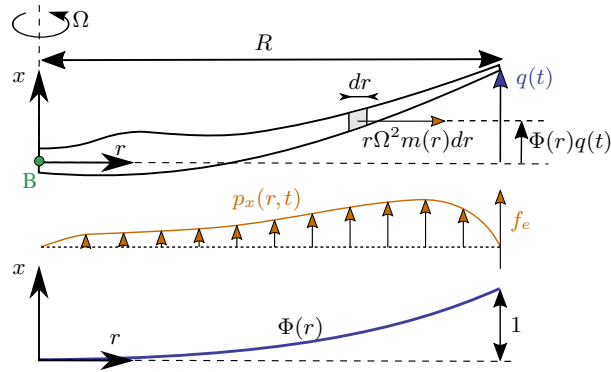


Figure 1. Sketch of a rotating blade, with the restoring centrifugal force. Points are indicated in green, degrees of freedom in blue, and loads in orange.

200 along the radial coordinate r , and rotates around the x axis. We assume that the shape function is known, noted $\Phi(r)$. It can
 201 be computed as the first flapwise mode of the blade, using tools provided in YAMS. The expression $\Phi(r) = r^3$ is a simple
 202 approximation that can be used for hand calculations. The aerodynamic force per length in the flapwise direction is noted
 203 $p_x(r)$. The generalized mass and stiffness are computed based on the mass per length (m) and flapwise bending stiffness (EI_y)
 204 of the blade, according to Equation B1:

$$206 \quad M_e = \int_0^R m(r)\Phi^2(r) dr \quad (26)$$

$$207 \quad K_e = \int_0^R EI_y(r) \left[\frac{d^2\Phi}{dr^2}(r) \right]^2 dr \quad (27)$$

208 The generalized force is obtained from Equation B3:

$$209 \quad f_e = \int_0^R p_x(r,t)\Phi(r) dr \quad (28)$$



210 The important consideration for this model is the axial load, N . The main axial load at a radial station r comes from the
 211 centrifugal force acting on all the points outboard of the current station:

$$212 \quad N(r) = \int_r^R m(r') \Omega^2 r' dr' \quad (29)$$

213 The geometrical stiffness contribution of the axial load is obtained from Equation B5 as:

$$214 \quad K_g(\Omega) = \int_0^R N(r) \left[\frac{d\Phi}{dr} \right]^2 dr = \Omega^2 \int_0^R \int_r^R m(r') r' dr' \left[\frac{d\Phi}{dr} \right]^2 dr \quad (30)$$

215 The axial stiffness, K_g , is positive and increases with the square of the rotational speed. This restoring effect is referred to as
 216 “centrifugal stiffening”. The natural frequency of the blade will increase with the rotational speed as follows:

$$217 \quad \omega_0(\Omega) = \sqrt{\frac{(K_e + K_g(\Omega))}{M_e}} = \sqrt{\omega_0^2(0) + \frac{K_g(\Omega)}{M_e}} = \sqrt{\omega_0^2(0) + k_\Omega \Omega^2} \quad (31)$$

218 where k_Ω is referred to as the rise factor, or Southwell coefficient, and in our approximation, it is found to be constant:
 219 $k_\Omega = K_g(\Omega)/M_e/\Omega^2$. The coefficient provides the variation of the blade frequency with rotational speed, which is something
 220 that is observed on a Campbell diagram when performing stability analyses. In general, the mode shapes of the blade will also
 221 change as function of the rotational speed, and different shape functions should preferably be used for simulations at different
 222 rotational speed. The effect is fairly limited, and most OpenFAST practitioners only use one shape function corresponding to
 223 the value at rated rotational speed. Similarly, the Southwell coefficient is a function of the rotational speed, but the variations
 224 is negligible as long as the rotational speed is small compared to the natural frequency (e.g., $(\Omega/\omega)^2 \lesssim 5$, see Bielawa (2006)),
 225 which is the case for wind energy applications.

226 The treatment for a shape function in the edgewise direction is similar, using $\Phi_2 = \Phi_2 \hat{\theta}$. In this case, the centrifugal force
 227 also has a component in the tangential direction equal to $p_{\theta, \text{centri}}(r) = -\Omega^2 u_\theta(r) dm(r)$, with $u_\theta = \Phi_2 q$. This leads to a gen-
 228 eralized force equal to $\int_0^L p_{\theta, \text{centri}} dr \Phi_2 = -\Omega^2 M_e q$, or equivalently, to a stiffness term: $K_\omega = -\Omega^2 M_e$. It can be verified that
 229 this generalized force corresponds to the contribution $O_{e,11} \omega_x^2$, from $\mathbf{k}_{\omega,e}$, given in Equation A10. For an edgewise mode, the
 230 frequency therefore evolves as:

$$231 \quad \omega_0(\Omega) = \sqrt{\frac{(K_e + K_g(\Omega) + K_\omega(\Omega))}{M_e}} = \sqrt{\omega_0^2(0) + (k_\Omega - 1)\Omega^2} \quad (32)$$

232 with $k_\Omega = K_g(\Omega)/M_e/\Omega^2$ and with K_g computed using Equation 30.

233 We apply the method to the NREL-5MW turbine using the blade properties and shape functions provided in the ElastoDyn
 234 input file. We order the degrees of freedom as: 1st flap, 1st edge and 2nd flap, assuming no coupling between the shape functions,
 235 so that they each of them can be treated individually using the results from this section. The diagonal coefficients of the mass
 236 matrix are $\text{diag}(\mathbf{M}_e) = [9.5e3, 1.5e4, 5.7e3]$, and for the stiffness matrix $\text{diag}(\mathbf{K}_e) = [1.7e4, 6.7e4, 8.7e4]$, computed ac-
 237 cording to Equation 26 and Equation 27. The coefficients k_Ω of each degrees of freedom are obtained as: $\mathbf{k}_\Omega = [1.7, 1.4, 5.5]$.

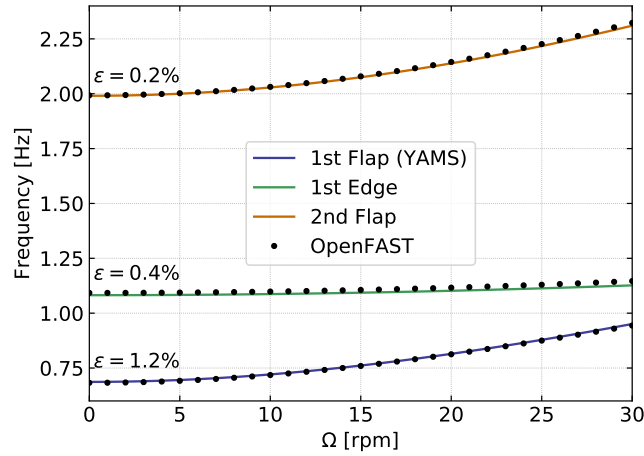


Figure 2. Variation of the natural frequencies of the NREL5-MW blade with rotational speed. Results from YAMS and OpenFAST, with mean relative error, ϵ , reported on the figure.

238 We compare the frequencies obtained with the present method against OpenFAST linearization results in Figure 2. The simu-
 239 lations were run in vacuum (no gravity, no aerodynamics) and with a cone angle of 0 deg. Strong agreement is found for the
 240 evolution of the different frequencies with the rotational speed. The stiffening is less pronounced for edgewise modes due to
 241 the softening introduced by K_ω .

242 This paragraph focused on the analysis of individual shape functions. In the general case, multiple shape functions are
 243 present and couplings might exist between them (due to the structural twist, non-orthogonality of the shape functions, or if the
 244 shape functions have components in multiple directions such as $\Phi_1 = \Phi_{1x}\hat{x} + \Phi_{1y}\hat{y}$). In such case, the general developments
 245 of Appendix A and Appendix B should be used.

246 4.4 Two degrees of freedom model of an onshore or fixed-bottom turbine

247 We consider a system of three bodies: tower (or support structure), nacelle and rotor. The system represents an onshore wind
 248 turbine or a fixed-bottom offshore wind turbine. A sketch of the system is given in Figure 3. The nacelle and rotor blades are
 249 rigid bodies, whereas the tower is flexible and represented by one shape function² in the fore-aft direction, noted $\Phi_1 = \Phi_1\hat{x}$.
 250 For hand calculations and as a first approximation, the first mode shape of a massless beam with a top-mass may be used:
 251 $\Phi_1(z) = 1 - \cos(z\pi/L/2)$. Increased accuracy is obtained when the shape function matches the actual first tower fore-aft
 252 bending mode accounting for the effect of the rotor-nacelle mass and inertia. The degrees of freedom are $q = (q, \psi)$, where
 253 q is the generalized (elastic) coordinates in the fore-aft direction and ψ is the azimuthal position. The slope of the tower
 254 shape function at the tower top is a key coupling parameter of the model, noted ν_y . When the tower deflects 1 m in the x
 255 direction, the nacelle rotates by an angle ν_y . The methods assumes that the tower-top point remains along the x axis, neglecting
 256 the so-called non-linear geometrical effect. Yet, non-linear geometrical effects can be included using geometrical stiffening

² The relevant equations of the shape function approach for a beam are given in Appendix B.

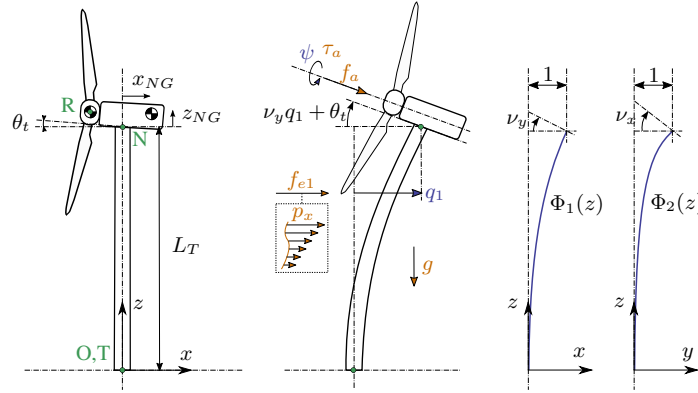


Figure 3. Model of an onshore or fixed-bottom wind turbine using 1 to 3 degrees of freedom (fore-aft and side-side flexibility of the support structure, and shaft rotation). Points are indicated in green, degrees of freedom in blue, and loads in orange.

257 corrections (Branlard, 2019). The aerodynamic thrust and torque are noted f_a , τ_a , acting at the rotor center (point R). The
 258 low-speed shaft generator torque is written τ_g . The distributed loads on the tower, p_x (from aero- and hydrodynamics), are
 259 projected against the shape function to obtain the generalized forces: $f_e = \int_0^{L_T} p_x(z, t) \Phi_1(z) dz$. The moments of inertia of the
 260 rotor in its coordinates are $(J_{x,R}, J_{\oplus,R}, J_{\ominus,R})$. We note M_e, K_e, D_e the generalized mass, stiffness and damping associated
 261 with a given shape function: $M_e = \int_0^{L_T} m(z) \Phi_1^2(z) dz$, $K_e = \int_0^{L_T} EI(z) \left[\frac{d^2 \Phi_1(z)}{dz^2} \right]^2 dz$, $D_e = 2\zeta M_e \omega_e$ where $m(z)$ and
 262 $EI(z)$ are the mass per length and bending stiffness of the tower, and ω_e and ζ are the frequency and damping ratio associated
 263 with the shape function (assuming the shape function is close to a mode shape). The geometrical softening of the tower due to
 264 the tower top mass (K_{gt}) and its self-weight (K_{gs}) is obtained using Equation B5, as $K_g = K_{gt} + K_{gs}$, with :

$$265 \quad K_{gt} = -g \int_0^{L_T} (M_R + M_N) \left[\frac{d\Phi_1(z)}{dz} \right]^2 dz \quad (33)$$

$$266 \quad K_{gs} = -g \int_0^{L_T} \left[\frac{d\Phi_1(z)}{dz} \right]^2 \left[\int_z^{L_T} m(z') dz' \right] dz \quad (34)$$

267 The shape function frequency is obtained as:

$$268 \quad \omega_e = \sqrt{(K_e + K_g)/M_e} \quad (35)$$

269 The application of the symbolic framework leads to the following equations of motion (rearranged for interpretability):

$$270 \quad \begin{bmatrix} M_q & 0 \\ 0 & J_{x,R} \end{bmatrix} \begin{bmatrix} \ddot{q} \\ \ddot{\psi} \end{bmatrix} = \begin{bmatrix} f_q \\ \tau_a - \tau_g \end{bmatrix} \quad (36)$$



271 where:

$$272 \quad M_q = M_e + M_N + M_R \quad (37)$$

$$273 \quad + (J_{yN} + J_{\oplus,R} + M_N(x_{NG}^2 + z_{NG}^2) + M_R(x_{NR}^2 + z_{NR}^2))\nu_y^2 \quad (38)$$

$$274 \quad + 2[(M_N z_{NG} + M_R z_{NR}) \cos(\nu_y q) - (M_N x_{NG} + M_R x_{NR}) \sin(\nu_y q)] \nu_y \quad (39)$$

275 and

$$276 \quad f_q = f_e - (K_e + K_g)q - D_e \dot{q} \quad (40)$$

$$277 \quad + g\nu_y [(M_N x_{NG} + M_R x_{NR}) \cos(\nu_y q) + (M_N z_{NG} + M_R z_{NR}) \sin(\nu_y q)] \quad (41)$$

$$278 \quad + \nu_y^2 \dot{q}^2 [(M_N x_{NG} + M_R x_{NR}) \cos(\nu_y q) + (M_N z_{NG} + M_R z_{NR}) \sin(\nu_y q)] \quad (42)$$

$$279 \quad + f_a \nu_y (x_{NR} \sin \theta_t + z_{NR} \cos \theta_t) \quad (43)$$

$$280 \quad + f_a \cos(\theta_t + \nu_y q) \quad (44)$$

281 Details on the derivations are given in Section D1. The mass matrix consists of three main contributions: Equation 37 represents
 282 the elastic mass and the rotor nacelle assembly (RNA) mass, Equation 38 is the generalized rotational inertia of the RNA,
 283 Equation 39 is the inertial coupling between the tower bending and the rotation of the nacelle. The forcing terms are identified as
 284 follows: Equation 40 consists of the elastic load due to the external forces on the tower, the elastic and geometric stiffness loads
 285 and the damping load on the tower; Equation 41 is the gravitational load from the RNA which will contribute to the stiffness of
 286 the system; Equation 42 is the centrifugal force of the RNA (“ $M\omega^2 r$ ” with $\omega = \nu_y \dot{q}$); Equation 43 is the generalized torque from
 287 the aerodynamic thrust and Equation 44 is the thrust contribution acting directly along the direction of the shape function degree
 288 of freedom (along x). The RNA center of mass plays an important part in the equations (see the terms $(M_N x_{NG} + M_R x_{NR})$
 289 and $(M_N z_{NG} + M_R z_{NR})$).

290 The equations of motion given in Equation 36 can be used to perform time domain simulations of a wind turbine. It is noted
 291 that the two degrees of freedom are only coupled by the aerodynamic loads. The non-linear model was used in previous work
 292 for time domain simulations and its linear version was used for state estimations (Branlard et al., 2020a, b). In this section, we
 293 apply the linearized form to compute the natural frequency of the turbine tower fore-aft mode. The linearized stiffness is here
 294 obtained by taking the gradient of the forcing with respect to q , and using a small angle approximation for ν_y to the second
 295 order:

$$296 \quad K_{q,lin} = (K_e + K_g) - \nu_y^2 (M_N g z_{NG} + M_R g z_{NR} - f_a q \cos \theta_t) + \nu_y f_a \sin \theta_t \quad (45)$$

297 For the NREL-5MW reference turbine (Jonkman et al., 2009), the different numerical values are: $g = 9.807 \text{ m.s}^{-2}$, $\theta_t = 5$
 298 deg, $x_{NR} = -5.0 \text{ m}$, $z_{NR} = 2.4 \text{ m}$, $L_T = 87.6 \text{ m}$, $z_{NG} = 1.75 \text{ m}$, $x_{NG} = 1.9 \text{ m}$, $M_R = 1.1e5 \text{ kg}$, $J_{x,R} = 3.86e7 \text{ kg m}^2$,
 299 $J_{\oplus,R} = 1.92e7 \text{ kg m}^2$, $M_N = 2.4e5 \text{ kg}$, $J_{y,N} = 1.01e6 \text{ kg m}^2$, $M_{RNA} = 3.5e5 \text{ kg}$. The first fore-aft shape function of the



300 NREL-5MW turbine tower, and its derivatives are:

$$\begin{aligned}
 301 \quad \Phi_1(z) &= (a_2 \bar{z}^2 + a_3 \bar{z}^3 + a_4 \bar{z}^4 + a_5 \bar{z}^5 + a_6 \bar{z}^6) / (a_2 + a_3 + a_4 + a_5 + a_6) \\
 302 \quad \frac{d\Phi_1}{dz}(z) &= \frac{1}{L_T} (2a_2 \bar{z} + 3a_3 \bar{z}^2 + 4a_4 \bar{z}^3 + 5a_5 \bar{z}^4 + 6a_6 \bar{z}^5) / (a_2 + a_3 + a_4 + a_5 + a_6) \\
 303 \quad \frac{d^2\Phi_1}{dz^2}(z) &= \frac{1}{L_T^2} (2a_2 + 6a_3 \bar{z} + 12a_4 \bar{z}^2 + 20a_5 \bar{z}^3 + 30a_6 \bar{z}^4) / (a_2 + a_3 + a_4 + a_5 + a_6)
 \end{aligned} \tag{46}$$

304 with $\bar{z} = z/L$ and $a_2 = 0.7004$, $a_3 = 2.1963$, $a_4 = -5.6202$, $a_5 = 6.2275$, $a_6 = -2.504$. The material properties and the shape function are illustrated in Figure 4. The scaling of the shape functions given in Equation 46 is important to obtain the correct

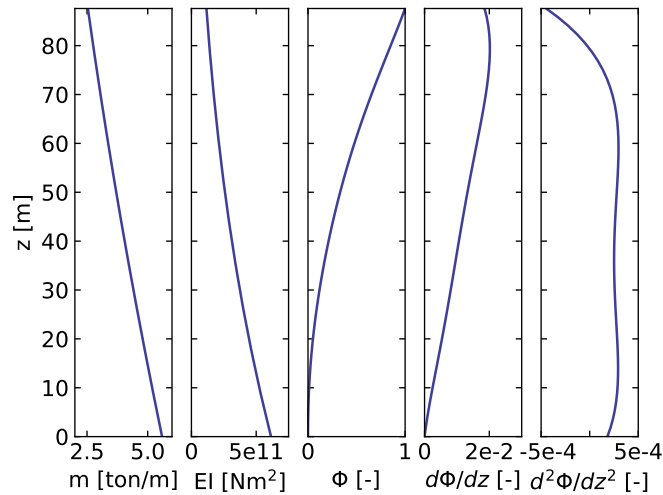


Figure 4. Properties of the NREL-5MW tower: mass per length (m), bending stiffness (EI), and shape function displacement (Φ), slope ($d\Phi/dz$) and curvature ($d^2\Phi/dz^2$).

305
 306 numerical values for the flexible tower, namely: $\nu_y = 0.0185$, $M_e = 5.4e4$, $K_e = 1.91e6$, $K_g = -5.2e4 - 1.0e4 = -6.20e4$,
 307 $\omega_e = \sqrt{(K_e + K_g)/M_e} = 5.85$ rad/s. These numerical values, with $q = 0$, leads to: $M_q = 4.375e5$ and $K_q = 1.849e9$. The
 308 first fore-aft mode of the wind turbine has a natural frequency of $f = \sqrt{K_q/M_q} = 0.3272$ Hz. This value was compared with
 309 results obtained using OpenFAST linearization. Both methods are in strong agreements with differences only arising at the
 310 fifth decimal place.

311 4.5 Three degrees of freedom model of an onshore or fixed-bottom turbine

312 We consider the same system as the one presented in subsection 4.4 but the tower is now represented by one shape function in
 313 both the fore-aft and side-side directions, $\Phi_1 = \Phi_1 \hat{x}$ and $\Phi_2 = \Phi_2 \hat{y}$. The degrees of freedom are $\mathbf{q} = (q_1, q_2, \psi)$, where q_1 and
 314 q_2 are the generalized (elastic) coordinates in the fore-aft and side-side directions respectively, and ψ is the rotor azimuth. A
 315 sketch of the system is given in Figure 3.



316 The slopes of the shape functions at the tower top are key coupling parameters of the model, noted ν_x and ν_y . The aerody-
 317 namic thrust and torque are noted f_a, τ_a , acting at point R . The distributed loads on the tower, p_x and p_y (from aero- and hydro-
 318 dynamics), are projected against the shape functions to obtain the generalized forces $f_{e1} = \int \Phi_1 p_x dz$ and $f_{e2} = \int \Phi_2 p_y dz$. The
 319 moments of inertia of the rotor in its coordinates are $(J_{x,R}, J_{\oplus,R}, J_{\ominus,R})$. We note M_e, K_e, D_e the generalized mass, stiffness
 320 and damping associated with a given shape function (e.g. $M_{e11} = \int \Phi_1^2 m(z) dz$, with m the mass per length of the tower). The
 321 application of the symbolic framework leads to the equations of motion given in Section D2. To simplify the equations and
 322 limit their length when printing them in this article, we have applied a first-order small angle approximation for θ_t , and second
 323 order for ν_x and ν_y . It is seen from Equation D14, that a first order approximation for ν_y would have removed the influence of
 324 the rotor and nacelle y -inertia on the generalized mass associated with the tower fore-aft bending.

325 We performed a time simulation of the model using both our symbolic framework YAMS and OpenFAST. We compare the
 326 time series obtained using our generated functions with results from the equivalent OpenFAST simulation in Figure 5. In this
 simulation, the tower top is initially displaced by 1 m in the x and y directions, and the rotational speed is 5 rpm. We report the

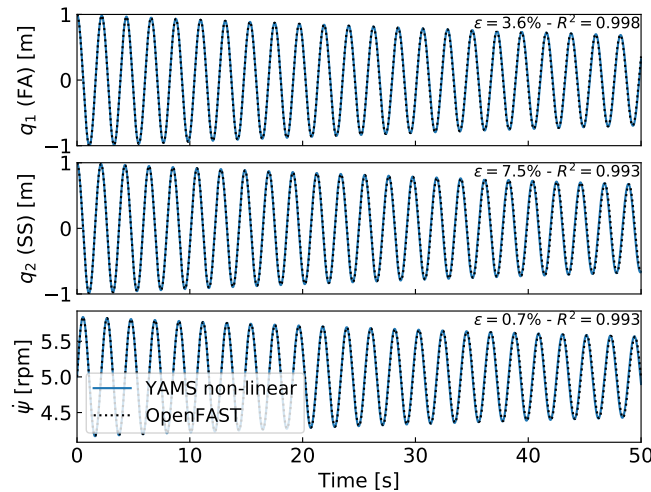


Figure 5. Free decay results for the onshore/fixed bottom model using both the symbolic framework (YAMS) and OpenFAST. From top to bottom: tower fore-aft bending, tower side side bending, and shaft rotational speed.

327 mean relative error, ϵ , and the coefficient of determination R^2 on the figure. We observe that our model is in strong agreement
 328 with the OpenFAST simulation. The differences in the second tower degree of freedom are attributed to: 1) the handling of the
 329 small angle approximation which is different in OpenFAST (using the closest orthonormal matrix, Jonkman (2009)) and in our
 330 formulation (two successive rotations, linearized); 2) the non-linear geometric corrections that are implemented in OpenFAST
 331 and which we have here omitted by only selecting shape function expansion to the first order (see subsection 5.3). The variation
 332 in azimuthal speed, resulting from the coupling between the gyroscopic loads and the tower bending, is well captured.
 333



334 4.6 Three degrees of freedom model of a floating turbine

335 In this example, we demonstrate the applicability of the method for a floating wind turbine. We model the turbine using 3
 336 bodies: rigid floater, flexible tower, rigid rotor-nacelle-assembly (labelled “N”). The degrees of freedom selected are: $\mathbf{q} =$
 337 (x, ϕ, q_T) , where x is the floater surge, ϕ , the floater pitch, and q_T , the coordinate associated with a selected fore-aft shape
 function. A sketch of the model is given in Figure 6. The notations are similar to the ones presented in subsection 4.5. Lumped

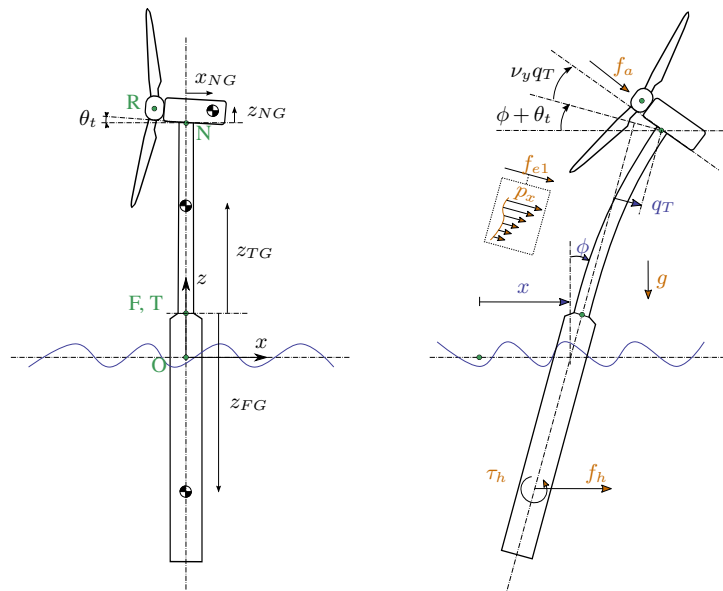


Figure 6. Model of an floating wind turbine using 3 degrees of freedom. Points are indicated in green, degrees of freedom in blue, and loads in orange.

338
 339 hydrodynamic loads at the floater center of mass are now added. The model can also be used for a combined tower and floater
 340 that is flexible, simply by setting the mass of the floater to zero and including the hydrodynamic loading into the loading p_x . The
 341 equations of motion are given in subsection D3. The equations were simplified using a first order small angle approximation
 342 of θ_t and ϕ_y , and a second order approximation for ν_y .

343 We performed a numerical simulation of the model generated by YAMS and compared it with OpenFAST, for a case with
 344 gravitational loads only, starting with $x = 0$ m, $\phi = 2$ deg and $q_T = 1$ m. The results are presented in Figure 7. We observe
 345 again that the results from the two models correlate to a high degree.

346 We also compared the linearized version of both models. The symbolic framework can generate the linearized mass, stiffness
 347 and damping matrices as described in subsection 2.5. The matrices are then combined into a state matrix and compared with
 348 the state matrices written by the OpenFAST linearization feature. The eigenvalue analysis of the YAMS state matrix returned
 349 a pitch and fore-aft frequencies of 0.099 Hz and 0.799 Hz respectively, whereas OpenFAST returned 0.095 Hz and 0.795 Hz.
 350 The 4% error in the pitch frequency appears reasonable in view of the approximations used.

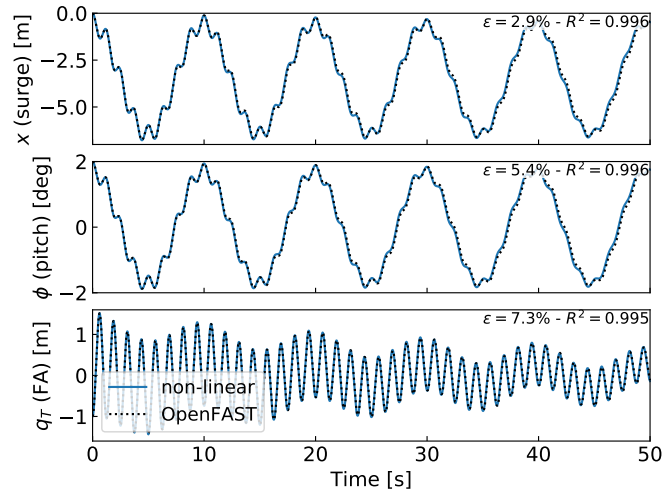


Figure 7. Free decay results for the floating wind turbine model using YAMS and OpenFAST. From top to bottom: surge, pitch and tower fore-aft bending.

351 5 Discussions

352 5.1 Applications

353 The implementation of the symbolic YAMS library was originally motivated by the need to obtain a simple linearized model
354 of a floating wind turbine for frequency domain simulations. The potential applications of the framework are yet multiple:

- 355 – The generated equations can be used in time-domain simulation tools. The equations can be readily exported to differ-
356 ent programming languages (C, Fortran or Python) providing computationally efficient tools, particularly because the
357 method generates compact, and minimal equations. This is in contrast to most other multibody codes where many terms
358 are calculated as matrix equations and through successive function calls. Further, the symbolic framework allows to
359 generate optimized code, where common terms and factors are computed once and stored in temporary variables for
360 reuse in the different expressions. In our examples, time-domain simulations were observed to be two orders of magni-
361 tude faster when using the automatically generated code in Python compared to OpenFAST simulations that rely on a
362 compiled-language. Using such a framework can be considered in the future to replace the existing ElastoDyn module
363 of OpenFAST. It can also be applied to unusual configurations such as multi-rotor or some vertical axis turbine concepts.
364 Dedicated code can be generated for specific applications for increased performances. For instance, implicit integrator
365 with iterative Newton-Raphson-like solvers benefit from the possibility to generate exact and efficient Jacobians along
366 with the equations of motion.
- 367 – The generation of linearized models have a wide range of applications, such as: linear time-domain simulations, con-
368 troller design and tuning, frequency domain analyses, stability analyses, state observers or digital twins. The symbolic



369 approach is severalfold faster than alternative approaches because it can be evaluated for all operating points at once,
370 whereas other methods (e.g. OpenFAST, HawcStab2) require multiple linearization calls. Linearization with respect to
371 parameters can also be performed, making the method even more appealing, e.g. for controller designs based on linear
372 parameter varying approaches such as linear matrix-inequality based designs (Pöschke et al., 2020).

373 – Analytical gradients of the equations can be computed and used in optimizations, nonlinear model predictive control
374 or moving horizon estimation. External loads that cannot be expressed analytically can be defined as generic functions
375 of the structural degrees of freedom, inputs, and parameters. After the code generation, the user can link a numerical
376 implementation of the function and its numerical gradients to be able to use a mix of analytical and numerical gradients.

377 **5.2 Advantage of using a symbolic framework**

378 Most advantages have already been discussed in subsection 5.1, namely: the wide range of applications and the potential gain
379 in computational time. Additionally, the method can provide useful insights and be used as an educational tool: simple models
380 of a system with few degrees of freedom can readily be obtained, studied, and compared to hand-based calculation.

381 **5.3 Advanced consideration**

382 Section 2 addressed the systematic derivation of the equations of motion for an assembly of rigid or flexible bodies. Some
383 advanced aspects of the method are discussed here:

384 – The expression of the displacement field \mathbf{u} in terms of a superposition of shape function is typically done using a first
385 or second order expansion. We discuss these formulations in Appendix C. Our framework supports both approaches: it
386 is the responsibility of the user to provide the terms and values of the expansion when numerical evaluation is to occur.
387 The advantage of the second-order expansion is that some geometrical non-linearities are directly accounted for by the
388 method, whereas these non-linearities need to be introduced “manually” in the first-order expansion approach, as done
389 in Branlard (2019).

390 – The definition of geometric stiffening requires attention in the general case. It is accounted for by the term \mathbf{k}_σ presented
391 in Appendix A. A general account of the effect for an arbitrary geometry can be found in Wallrapp and Schwertassek
392 (1991) and simplified expressions are given for beams in Appendix B.

393 – The treatment of external loads was not addressed in details in this paper because the loads are application specific (aero-
394 dynamics, hydrodynamics, etc.). The framework can accept external loads as arbitrary functions of multiple variables,
395 or as analytical expressions. In the former case, the user will have to provide an implementation of the function during
396 the execution.

397 – Even though the equations of motion are void of constraint forces, the values of these forces can be recovered. They
398 can be expressed as function of the external forces and the states of the system. It is not necessary to compute them by
399 iteratively solving constraint equations.



400 – The framework can easily include rheonomous constraints, e.g. for the pitch angle, without having to supply a dedicated
401 torque. Pitch speed and accelerations can be directly introduced into the mechanical system if they are provided e.g. by
402 a generic second order pitch actuator model

403 **5.4 Limitations**

404 In spite of the advantages listed in subsection 5.2, the symbolic procedure presented in this work has some potential limitations.
405 We are identifying two in this section. First, constraints and closed loops have currently not been added to the framework. The
406 SymPy mechanics package supports additional constraint equations within the Kane method. It is therefore hoped that this
407 current limitation can be lifted in the future. Second, large problems may challenge a symbolic calculation package: memory
408 impact, calculation time, simplification times, and size of expressions may become significant. Some of these issues may be
409 alleviated by introducing intermediate variables that are only substituted for in the numerical implementation or by using a
410 recursive formulation of the solution procedure (Branlard, 2019).

411 **6 Conclusions**

412 We presented a symbolic framework to obtain the linear and non-linear equations of motion of a multibody system made of
413 rigid bodies, flexible bodies and kinematic joints. Our approach is based on Kane's method and a nonlinear shape function
414 representation of flexible bodies. We provided different wind energy examples and verified the results against OpenFAST sim-
415 ulations. The framework can readily provide models suitable to a wide range of applications, with competitive computational
416 times. The framework is opensource and the examples presented are available in the repository. Future work will focus on
417 applying the framework to dedicated research projects, with more complex systems, and potentially extend the framework to
418 account for closed-loop systems and arbitrary constraints.

419 *Author contributions.* Both authors exchanged over the last two years on the implementation of such framework and its application to wind
420 energy. E. Branlard wrote a Python implementation and J. Geisler wrote a Maxima implementation. E. Branlard wrote the main corpus of
421 the paper, with feedback and contributions from J. Geisler.

422 *Competing interests.* No competing interests are present.

423 **Appendix A: Equations for a flexible body and shape integrals**

424 In this section, we detail the equations of motion of a flexible body. The reader is referred to the following references for a
425 complete treatment of the equations of motion: Shabana (2013), Schwertassek and Wallrapp (1999) and Wallrapp (1994). The
426 subscript i indicating the body index is dropped. The number of flexible shape functions associated with the body is n_e , the



427 flexible degrees of freedom are \mathbf{q}_e , and the shape functions are gathered into a matrix Φ of size $(3 \times n_e)$. Primes are used
 428 to indicate that quantities are expressed in the body frame of reference. The equations of motion, given in Equation 11, are
 429 repeated below:

$$430 \begin{bmatrix} M'_{xx} & M'_{x\theta} & M'_{xe} \\ & M'_{\theta\theta} & M'_{\theta e} \\ \text{sym.} & & M'_{ee} \end{bmatrix}_i \begin{bmatrix} \mathbf{a}'_i \\ \dot{\boldsymbol{\omega}}_i \\ \ddot{\mathbf{q}}_{e,i} \end{bmatrix} + \begin{bmatrix} \mathbf{k}'_{\omega,x} \\ \mathbf{k}'_{\omega,\theta} \\ \mathbf{k}_{\omega,e} \end{bmatrix}_i + \begin{bmatrix} 0 \\ 0 \\ \mathbf{k}_e \end{bmatrix}_i = \begin{bmatrix} \mathbf{f}'_x \\ \mathbf{f}'_\theta \\ \mathbf{f}_e \end{bmatrix}_i \quad (\text{A1})$$

431 The different terms of the mass matrix are obtained as follows:

$$432 M'_{xx} = \int \mathbf{I}_3 dm = M \mathbf{I}_3 \quad (3 \times 3) \quad (\text{A2})$$

$$433 M'_{x\theta} = - \int \tilde{\mathbf{s}}'_P dm = -M \tilde{\mathbf{s}}'_{CM} \quad (3 \times 3) \quad (\text{A3})$$

$$434 M'_{\theta\theta} = - \int \tilde{\mathbf{s}}'_P \tilde{\mathbf{s}}'_P dm = \mathbf{J} \quad (3 \times 3) \quad (\text{A4})$$

$$435 M'_{\theta e} = \int \tilde{\mathbf{s}}'_P \Phi' dm = \mathbf{C}_r^T \quad (3 \times n_e) \quad (\text{A5})$$

$$436 M'_{xe} = \int \Phi' dm = \mathbf{C}_t^T \quad (3 \times n_e) \quad (\text{A6})$$

$$437 M'_{ee} = \int \Phi'^T \Phi' dm \quad (n_e \times n_e) \quad (\text{A7})$$

438 The integrals are understood as volume integrals over the volume of the body (for beams they reduce to line integrals). The
 439 notation $[\tilde{\cdot}]$ represents the skew symmetric matrix. M is the mass of the body. The vector \mathbf{s}'_{CM} is the vector from the origin of
 440 the body to undeflected center or mass (CM) of the body. The notations \mathbf{C}_t ($n_e \times 3$) and \mathbf{C}_r ($n_e \times 3$) are introduced to match
 441 Wallrapp's notations. The vector \mathbf{s}'_P is the vector from the origin of the body to a deflected point of the body of elementary
 442 mass dm . The undeflected position of this point is written \mathbf{s}'_{P_0} and the displacement field \mathbf{u}' , such that: $\mathbf{s}'_P = \mathbf{s}'_{P_0} + \mathbf{u}'$. For
 443 a first order expansion of the displacement field, $\mathbf{u}' = \Phi' \mathbf{q}_e$. Second order expansions need the introduction of an additional
 444 notation: $\mathbf{u}' = \Phi'_u(\mathbf{q}_e) \mathbf{q}_e$ (see subsection 5.3 and Wallrapp (1994)). Wallrapp also includes the elementary mass moment of
 445 inertia which results in additional terms in the integrals (see Wallrapp (1994)). Such contributions are relevant for instance
 446 when considering the torsion of a beam (see Branlard (2019)). The block matrices M'_{xx} , M'_{xe} and M'_{ee} do not depend on
 447 the deformation of the body and are hence constant. The other terms are functions of \mathbf{q}_e . They may be expressed as linear
 448 combination of constant integrals. These integrals are usually referred to as shape integrals (Shabana (2013)) or Taylor series
 449 coefficients (Wallrapp (1994)).



450 The quadratic velocity terms \mathbf{k}_ω are given as:

$$451 \quad \mathbf{k}'_{\omega,x} = 2\tilde{\omega}' \mathbf{C}'_t \dot{\mathbf{q}}_e + M \tilde{\omega}' \tilde{\omega}' s'_{CM} \quad (3 \times 1) \quad (\text{A8})$$

$$452 \quad \mathbf{k}'_{\omega,\theta} = \tilde{\omega}' M'_{\theta\theta} \omega' + \left[\sum_{j=1..n_e} \mathbf{G}_{r,j} \dot{q}_{e,j} \right] \omega' \quad (3 \times 1) \quad (\text{A9})$$

$$453 \quad \mathbf{k}_{\omega,e} = [\omega'^T \mathbf{O}_{e,j} \omega']_{j=1..n_e} + \left[\sum_{j=1..n_e} \mathbf{G}_{e,j} \dot{q}_{e,j} \right] \omega' \quad (n_e \times 1) \quad (\text{A10})$$

454 where

$$455 \quad \mathbf{G}_{r,j} = -2 \int \tilde{s}'_P \tilde{\Phi}'_j dm \quad (3 \times 3) \quad (\text{A11})$$

$$456 \quad \mathbf{O}_{e,j} = \int \tilde{\Phi}'_j \tilde{s}'_P dm = -\frac{1}{2} \mathbf{G}'_{r,j} \quad (3 \times 3) \quad (\text{A12})$$

$$457 \quad \mathbf{G}_{e,j} = -2 \int \tilde{\Phi}'^T \tilde{\Phi}'_j dm \quad (n_e \times 3) \quad (\text{A13})$$

458 The first term of Equation A10 is obtained by vertically stacking the contribution of each shape function. In the SID format,
 459 this term is reshaped as the product $\mathbf{O}_e \boldsymbol{\Omega}$, where:

$$460 \quad \mathbf{O}_e = [O_{e,j,11}, O_{e,j,22}, O_{e,j,33}, O_{e,j,12} + O_{e,j,21}, O_{e,j,23} + O_{e,j,32}, O_{e,j,13} + O_{e,j,31}]_{j=1..n_e} \quad (n_e \times 6) \quad (\text{A14})$$

$$461 \quad \boldsymbol{\Omega} = [\omega_x^2, \omega_y^2, \omega_z^2, \omega_x \omega_y, \omega_y \omega_z, \omega_x \omega_z]^T \quad (6 \times 1) \quad (\text{A15})$$

462 The body elastic forces are given by:

$$463 \quad \mathbf{k}_e = \mathbf{k}_\sigma + \mathbf{K}_e \mathbf{q}_e + \mathbf{D}_e \dot{\mathbf{q}}_e \quad (\text{A16})$$

464 where \mathbf{K}_e and \mathbf{D}_e are the elastic stiffness and damping matrix, and \mathbf{k}_σ represent stress stiffening terms. The elastic damping
 465 forces are often given as stiffness proportional damping. For more details, see Wallrapp (1994), and for more example of with
 466 elastic beams see Branlard (2019). The external loads can be assumed to consists of distributed volume forces \mathbf{p}' (in practice
 467 they are mostly surface forces of line forces) and a gravitational acceleration field \mathbf{g}' . The components of the external loads in
 468 Equation A1 are then obtained by integration over the whole body:

$$469 \quad \mathbf{f}'_x = \int \mathbf{p}' dV + M'_{xx} \mathbf{g}' \quad (3 \times 1) \quad (\text{A17})$$

$$470 \quad \mathbf{f}'_\theta = \int s'_P \times \mathbf{p}' dV + M'_{\theta x} \mathbf{g}' \quad (3 \times 1) \quad (\text{A18})$$

$$471 \quad \mathbf{f}'_e = \int \tilde{\Phi}'^T \mathbf{p}' dV + M'_{ex} \mathbf{g}' \quad (n_e \times 1) \quad (\text{A19})$$

472 Appendix B: Application of the shape function approach to an isolated beam

473 In this section, we illustrate how the elastic equations of Appendix A can be applied to an isolated beam. Examples of ap-
 474 plications are further given in subsection 4.3 and subsection 4.4. We consider a beam directed along the z -axis and bend-



475 ing in the x and y direction. Expression are written in the coordinate system of the beam and primes are dropped in this
 476 section. The beam properties are the following: length L , mass per length m , and bending stiffness EI_x and EI_y . We as-
 477 sume that the displacement field is such that the shape functions are function of z only: $\mathbf{u}(z, t) = \sum_{i=1}^{n_e} \Phi_i(z) q_{e,i}(t)$. We
 478 also assume that the shape functions satisfy at least the geometric boundary conditions. The kinetic energy of the beam is
 479 $T = \frac{1}{2} \int_0^L m \dot{\mathbf{u}}^2 dz = \frac{1}{2} \sum_i \sum_j M_{e,ij} \dot{q}_{e,j} \dot{q}_{e,i}$, where $M_{e,ij}$ is (see Equation A7):

$$480 \quad M_{e,ij} = \int_0^L m(z) \Phi_i(z) \cdot \Phi_j(z) dz, \quad i, j = 1, \dots, n_e \quad (\text{B1})$$

481 Equation B1 involves a scalar product of the shape functions at each spanwise positions. Integrals over the moment of inertia
 482 can be used to account for torsion (see Branlard (2019)). The potential energy (strain energy) of the beam, is obtained as $V =$
 483 $\frac{1}{2} \sum_i \sum_j K_{e,ij} q_{e,i} q_{e,j}$, where $K_{e,ij}$ are the element of the stiffness matrix, which, under the assumption of small deformations,
 484 are given by:

$$485 \quad K_{e,ij} = \int_0^L \left[EI_y \frac{d^2 \Phi_{i,x}}{dz^2} \frac{d^2 \Phi_{j,x}}{dz^2} + EI_x \frac{d^2 \Phi_{i,y}}{dz^2} \frac{d^2 \Phi_{j,y}}{dz^2} \right] dz, \quad i, j = 1, \dots, n_e \quad (\text{B2})$$

486 Elongation and torsional strains (EA and GK_t) can similarly be added to the strain energy and the stiffness matrix if longi-
 487 tudinal and torsional displacement fields are included in the shape functions. The external loads on the beam are assumed to
 488 consist of a distributed force vector $\mathbf{p}(z)$. The virtual work done by the force \mathbf{p} for each virtual displacement $\delta q_{e,i}$, provides
 489 the generalized force as(see Equation A17):

$$490 \quad f_{e,i} = \int_0^L \Phi_i \cdot \mathbf{p} dz \quad (\text{B3})$$

491 The equations of motion of the isolated beam and then written in matricial form as:

$$492 \quad \mathbf{M}_e \ddot{\mathbf{q}}_e + \mathbf{D}_e \dot{\mathbf{q}}_e + \mathbf{K}_e \mathbf{q}_e = \mathbf{f}_e \quad (\text{B4})$$

493 where $\mathbf{q}_e = [q_{e,1}, \dots, q_{e,n}]$. Damping is typically added a posteriori to the equations, where the Rayleigh damping assumption
 494 is often used $\mathbf{D}_e = \alpha \mathbf{M}_e + \beta \mathbf{K}_e$ (stiffness proportional damping implies $\alpha = 0$). If the shape functions are mode shapes, then
 495 the shape functions are orthogonal, the mass and stiffness matrices are diagonal, and the stiffness values would be $K_{e,ii} =$
 496 $\omega_{e,i}^2 M_{e,ii}$, with $\omega_{e,i} = \sqrt{K_{e,ii}/M_{e,ii}}$ the eigenfrequency of the beam mode i . The modal damping is then given by $D_{e,ii} =$
 497 $2\zeta_i M_{e,ii} \omega_{e,i}$, where ζ_i is the damping ratio associated with mode i .

498 If the beam is loaded axially by a force $N(z)$, then this force produces a distributed load in the transverse direction equal
 499 to $\mathbf{n} = \frac{\partial}{\partial z} [N(z) \frac{\partial \mathbf{u}}{\partial z}]$, with components in the y and z directions (see Branlard (2019)). The generalized force associated with
 500 this loading is then: $Q_{N,i} = \int_0^L \Phi_i \cdot \mathbf{n} dz$. Inserting the expression of \mathbf{n} and \mathbf{u} , the generalized force has the form of a stiffness
 501 term: $Q_{N,i} = - \sum_j K_{N,ij} q_j$ with

$$502 \quad K_{N,ij} = - \int_0^L \Phi_i \cdot \frac{d}{dz} \left[N(z) \frac{d\Phi_j}{dz} \right] dz = \int_0^L N(z) \frac{d\Phi_i}{dz} \cdot \frac{d\Phi_j}{dz} - \left[N(x) \Phi_i \cdot \frac{d\Phi_j}{dz} \right]_0^L \quad (\text{B5})$$



503 and where integration by parts was used to obtain the second equality. Examples of applications are given in subsection 4.3
 504 and subsection 4.4.

505 **Appendix C: Alternative formulations**

506 Different formulations of flexible multibody dynamics are found in the literature. Some of the alternatives are briefly discussed
 507 in this section.

508 In Equation 7, the Jacobian terms \mathbf{J} and the virtual work are expressed in vector form. In such form, there is no need to
 509 precise in which coordinate system the different vectors are expressed. This is convenient to reduce the size of the expressions
 510 when using symbolic calculations. In a numerical framework, the vector will have to be expressed in a common frame. When
 511 such approach is used (see e.g. Lemmer (2018); Branlard (2019)), the Jacobians are sometimes stacked into a matricial form:

$$512 \quad \mathbf{J} = \begin{bmatrix} \mathbf{J}_v \\ \mathbf{J}_\omega \\ \mathbf{J}_e \end{bmatrix} \quad (C1)$$

513 Some implementation choices are needed depending if these matrices are expressed in the global frame or a body frame. The
 514 Jacobian matrices are referred to as velocity transformation matrix, and the link between formulations in global and local
 515 coordinates is given in Branlard (2019). In the same reference, recursive relationships are given for tree-like assembly of
 516 bodies, to help express the Jacobian matrices of each body recursively, based on the matrices of the parent body. It is also noted
 517 that the quadratic velocity terms, \mathbf{k}_ω , can be obtained using the time derivative of the Jacobian matrix.

518 In this article, we have not explicitly written the rotational impact of the shape functions. In most applications, bodies are
 519 connected at their extremities and the deflection slope at a body extremity will induce a rotation of the subsequent body. The
 520 deflection slope can be obtained from the knowledge of the shape functions. This is readily accounted for by introducing time-
 521 varying rotation matrix between bodies, and this is the approach used in our symbolic framework. A formalism of rotations
 522 of bodies connected at their extremities is given in Branlard (2019). A more general formulation, introducing shape function
 523 rotations Ψ , is given in (Wallrapp, 1994; Schwertassek and Wallrapp, 1999; Lemmer, 2018). In such formulation, the linear
 524 rotation field is obtained as $\mathbf{I} + \widetilde{\Psi}\mathbf{q}$, where \mathbf{I} is the identity matrix.

525 The order of expansion of the displacement field leads to alternative formulations. In Shabana (2013) and Branlard (2019) a
 526 first order expansion is used: $\mathbf{u} = \sum_j [\Phi_j^0] q_{e,j}$ In the work of Wallrapp a second order expansion is used: $\mathbf{u} = \sum_j [\Phi_j^0 + \frac{1}{2} \sum_k \Phi_{jk}^1 q_{e,k}] q_{e,j}$
 527 In both formulations, the equations of motion given in Appendix A lead to shape-integral expansions of the following form:

$$528 \quad \mathbf{T} = \mathbf{T}^0 + \sum_{j=1..n_e} \mathbf{T}_j^1 q_{e,j} \quad (C2)$$

529 where \mathbf{T} is a dummy variable standing for $M_{\theta,\theta}$, C_t , C_r , G_r , G_e , or O_e . The “0” and “1” terms are stored using a “Taylor”
 530 object-oriented class in the SID format defined by Wallrapp. The subtlety lays in the fact that the “1” terms will be different
 531 if the displacement is developed using a first order expansion or a second order expansion. Some terms involving Φ_{jk}^1 will be



532 present in the latter case. The reader is referred to Wallrapp (1993) for a full description of the Taylor-expanded terms. Setting
 533 $\Phi_{jk}^1 = 0$ in these expressions will lead to the 1st-order shape integral approach of Shabana.

534 Appendix D: Equations of motion of simple wind turbine models

535 D1 Three degrees of freedom model of an onshore or fixed-bottom wind turbine

536 In this section we provide some intermediate values to obtain the equations of motion given in subsection 4.4. The degrees of
 537 freedom are $q = (q, \psi)$. The kinematics of the tower (at its origin) are zero:

$$538 \mathbf{v}_{O,T} = \mathbf{0}, \quad \boldsymbol{\omega}_T = \mathbf{0}, \quad \mathbf{a}_{O,T} = \mathbf{0} \quad (\text{D1})$$

539 All Jacobians are zero except $\mathbf{J}_{e,1T} = 1$ The inertial force, torque and elastic force are:

$$540 \mathbf{f}_T^* = C_{tTx} \ddot{q} \hat{\mathbf{t}}_x + M_T g \hat{\mathbf{t}}_z, \quad \boldsymbol{\tau}_T^* = C_{rTy} \ddot{q} \hat{\mathbf{t}}_y, \quad \mathbf{E}_T^* = f_e + D_e \dot{q} + (K_e + K_q)q + M_e \ddot{q} \quad (\text{D2})$$

541 The nacelle kinematics (at its center of mass) are:

$$542 \mathbf{v}_{G,N} = \dot{q} \hat{\mathbf{t}}_x + \nu_y z_{NG} \dot{q} \hat{\mathbf{n}}_x - \nu_y x_{NG} \dot{q} \hat{\mathbf{n}}_z, \quad \boldsymbol{\omega}_N = \nu_y \dot{q} \hat{\mathbf{t}}_y \quad (\text{D3})$$

$$543 \mathbf{a}_{G,N} = \ddot{q} \hat{\mathbf{t}}_x + (-\nu_y^2 x_{NG} \dot{q}^2 + \nu_y z_{NG} \ddot{q}) \hat{\mathbf{n}}_x + (-\nu_y^2 z_{NG} \dot{q}^2 - \nu_y x_{NG} \ddot{q}) \hat{\mathbf{n}}_z \quad (\text{D4})$$

544 The Jacobians with respect to q are:

$$545 \mathbf{J}_{v,1N} = \hat{\mathbf{t}}_x + \nu_y z_{NG} \hat{\mathbf{n}}_x - \nu_y x_{NG} \hat{\mathbf{n}}_z, \quad \mathbf{J}_{\omega,1N} = \nu_y \hat{\mathbf{t}}_y \quad (\text{D5})$$

546 The inertial force and torque on the nacelle are:

$$547 \mathbf{f}_N^* = M_N \ddot{q} \hat{\mathbf{t}}_x + M_N (-\nu_y^2 x_{NG} \dot{q}^2 + \nu_y z_{NG} \ddot{q}) \hat{\mathbf{n}}_x + M_N (-\nu_y^2 z_{NG} \dot{q}^2 - \nu_y x_{NG} \ddot{q}) \hat{\mathbf{n}}_z, \quad \boldsymbol{\tau}_N^* = J_{y,N} \nu_y \ddot{q} \hat{\mathbf{n}}_y \quad (\text{D6})$$

548 The kinematics of the rotor are:

$$549 \mathbf{v}_{G,R} = \dot{q} \hat{\mathbf{t}}_x + \nu_y z_{NR} \dot{q} \hat{\mathbf{n}}_x - \nu_y x_{NR} \dot{q} \hat{\mathbf{n}}_z, \quad \boldsymbol{\omega}_R = \dot{\psi} \hat{\mathbf{e}}_{rx} + \nu_y \dot{q} \hat{\mathbf{t}}_y \quad (\text{D7})$$

$$550 \mathbf{a}_{G,R} = \ddot{q} \hat{\mathbf{t}}_x + (-\nu_y^2 x_{NR} \dot{q}^2 + \nu_y z_{NR} \ddot{q}) \hat{\mathbf{n}}_x + (-\nu_y^2 z_{NR} \dot{q}^2 - \nu_y x_{NR} \ddot{q}) \hat{\mathbf{n}}_z \quad (\text{D8})$$

551 The corresponding Jacobians with respect to q (“1”) and ψ (“2”) are:

$$552 \mathbf{J}_{v,1R} = \hat{\mathbf{t}}_x + \nu_y z_{NR} \hat{\mathbf{n}}_x - \nu_y x_{NR} \hat{\mathbf{n}}_z, \quad \mathbf{J}_{\omega,1R} = \nu_y \hat{\mathbf{t}}_y, \quad \mathbf{J}_{\omega,2R} = \hat{\mathbf{r}}_x$$

553 The inertial force and torque on the rotor are:

$$554 \mathbf{f}_R^* = M_R \ddot{q} \hat{\mathbf{t}}_x + M_R (-\nu_y^2 x_{NR} \dot{q}^2 + \nu_y z_{NR} \ddot{q}) \hat{\mathbf{n}}_x + M_R (-\nu_y^2 z_{NR} \dot{q}^2 - \nu_y x_{NR} \ddot{q}) \hat{\mathbf{n}}_z \quad (\text{D9})$$

$$555 \boldsymbol{\tau}_R^* = J_{x,R} \dot{\psi} \hat{\mathbf{r}}_x \quad (\text{D10})$$

$$556 + (J_{\oplus,R} \nu_y \sin(\psi) \dot{\psi} \dot{q} + J_{\ominus,R} (-\nu_y \sin(\psi) \dot{\psi} \dot{q} + \nu_y \cos(\psi) \ddot{q})) - J_{x,R} \nu_y \sin(\psi) \dot{\psi} \dot{q} \hat{\mathbf{r}}_y \quad (\text{D11})$$

$$557 + (J_{\oplus,R} \nu_y \cos(\psi) \dot{\psi} \dot{q} + J_{\ominus,R} (-\nu_y \sin(\psi) \ddot{q} - \nu_y \cos(\psi) \dot{\psi} \dot{q})) - J_{x,R} \nu_y \cos(\psi) \dot{\psi} \dot{q} \hat{\mathbf{r}}_z \quad (\text{D12})$$



558 **D2 Three degrees of freedom model of an onshore or fixed-bottom wind turbine**

559 The equations of motion for the model presented in subsection 4.5, with $\mathbf{q} = (q_1, q_2, \psi)$, are given in this section. The elements
 560 of the mass matrix are:

561 $M_{11} = [M_{e11} + M_N + M_R]$ (D13)

562 $+ [J_{y,N} + J_{\oplus,R} + M_N (x_{NG}^2 - 2x_{NG}q_1 + z_{NG}^2) + M_R (x_{NR}^2 - 2x_{NR}q_1 + z_{NR}^2)] \nu_y^2$ (D14)

563 $+ 2[M_N z_{NG} + M_R z_{NR}] \nu_y$ (D15)

564 $M_{13} = J_{x,R} \theta_t \nu_x \nu_y q_2$ (D16)

565 $M_{22} = [M_{e22} + M_N + M_R]$ (D17)

566 $+ [J_{x,N} + J_{x,R} + M_N z_{NG}^2 + M_R z_{NR}^2] \nu_x^2$ (D18)

567 $- 2[M_N z_{NG} + M_R z_{NR}] \nu_x$ (D19)

568 $M_{23} = J_{x,R} \nu_x$ (D20)

569 $M_{33} = J_{x,R}$ (D21)

570 The elements of the forcing vector are:

571 $f_1 = f_{e1} - K_{e11} q_1 - D_{e11} \dot{q}_1 - J_{x,R} \theta_t \nu_x \nu_y \dot{\psi} \dot{q}_2 + [M_N x_{NG} + M_R x_{NR}] \nu_y^2 \dot{q}_1^2$ (D22)

572 $+ g [M_N (\nu_y^2 z_{NG} q_1 + \nu_y x_{NG}) + M_R (\nu_y^2 z_{NR} q_1 + \nu_y x_{NR})] + f_a [\theta_t \nu_y x_{NR} - \theta_t \nu_y q_1 + \nu_y z_{NR} + 1]$ (D23)

573 $f_2 = f_{e2} - K_{e22} q_2 - D_{e22} \dot{q}_2 + J_{x,R} \theta_t \nu_x \nu_y \dot{\psi} \dot{q}_1$ (D24)

574 $+ g [M_N z_{NG} + M_R z_{NR}] \nu_x^2 q_2 + f_a \theta_t \nu_x q_2$ (D25)

575 $f_3 = -J_{x,R} \theta_t \nu_x \nu_y \dot{q}_1 \dot{q}_2 + \tau_a$ (D26)

576 **D3 Three degrees of freedom model of a floating wind turbine**

577 The equations of motion for the model presented in subsection 4.6, with $\mathbf{q} = (x, \phi, q_T)$, are given in this section. The elements
 578 of the mass matrix are:

579 $M_{11} = M_F + M_T + M_N$ (D27)

580 $M_{12} = M_F z_{FG} - M_{dTz} + M_N [L_T + z_{NG} - \nu_y x_{NG} q_T - \phi_y (x_{NG} + q_T + \nu_y z_{NG} q_T)]$ (D28)

581 $M_{13} = C_{tT1x} + M_N [1 + \nu_y z_{NG} - \nu_y^2 x_{NG} q_T - \phi_y (\nu_y^2 z_{NG} q_T + \nu_y x_{NG})]$ (D29)

582 $M_{22} = J_{y,F} + M_F z_{FG}^2 + J_{T,y} + J_{y,N} + M_N [(L_T^2 + z_{NG}^2) + (q_T + x_{NG})^2 + 2\nu_y q_T (z_{NG} q_T - L_T x_{NG})]$ (D30)

583 $M_{23} = C_{rT1y} + [J_{y,N} + M_N (x_{NG}^2 + z_{NG}^2 + L_T z_{NG} + \nu_y q_T (z_{NG} q_T - L_T x_{NG}))] \nu_y + M_N [L_T + z_{NG}]$ (D31)

584 $M_{33} = M_e + M_N + [J_{y,N} + M_N (x_{NG}^2 - 2x_{NG} q_T + z_{NG}^2)] \nu_y^2 + 2M_N \nu_y z_{NG}$ (D32)



585 The elements of the forcing vector are:

$$586 \quad f_1 = f_H + [M_F z_{FG} - M_{dz} + M_N(L_T + z_{NG} - \nu_y x_{NG} q_T)] \phi_y \dot{\phi}_y^2 + M_N [q_T + x_{NG} + \nu_y z_{NG} q_T] \dot{\phi}_y^2 \quad (D33)$$

$$587 \quad + [2C_{tx} + M_N(1 + \nu_y z_{NG} - \nu_y^2 x_{NG} q_T)] \phi_y \dot{\phi}_y \dot{q}_T + M_N \nu_y [x_{NG} + \nu_y z_{NG} q_T] \dot{\phi}_y \dot{q}_T \quad (D34)$$

$$588 \quad + M_N \nu_y^2 [x_{NG} + z_{NG} \phi_y] \dot{q}_T^2 \quad (D35)$$

$$589 \quad + f_a [1 - \theta_t \nu_y q_T - \nu_y \phi_y q_T] \quad (D36)$$

$$590 \quad f_2 = \tau_H + M_N [\nu_y^2 (L_T x_{NG} - z_{NG} q_T)] \dot{q}_T^2 \quad (D37)$$

$$591 \quad - 2M_N [q_T + x_{NG} + \nu_y (2z_{NG} q_T - L_T x_{NG}) - \nu_y^2 q_T (L_T z_{NG} + x_{NG} q_T)] \dot{\phi}_y \dot{q}_T \quad (D38)$$

$$592 \quad + g [M_F z_{FG} \phi_y - M_{dz} \phi_y + M_N \{(L_T + z_{NG} - \nu_y x_{NG} q_T) \phi_y + q_T + x_{NG} + \nu_y z_{NG} q_T\}] \quad (D39)$$

$$593 \quad + f_a [L_T + z_{NR} + \theta_t x_{NR} + \theta_t q_T + \nu_y q_T^2 - L_T \theta_t \nu_y q_T] \quad (D40)$$

$$594 \quad f_3 = f_e - D_e \dot{q}_T - K_e q_T \quad (D41)$$

$$595 \quad + M_N [q_T + x_{NG} + \nu_y (2z_{NG} q_T - L_T x_{NG}) - \nu_y^2 q_T (L_T z_{NG} + x_{NG} q_T)] \dot{\phi}_y^2 \quad (D42)$$

$$596 \quad + M_N \nu_y^2 x_{NG} \dot{q}_T^2 \quad (D43)$$

$$597 \quad + g [C_{tT1x} \phi_y + M_N (\nu_y x_{NG} + \nu_y^2 z_{NG} q_T - \nu_y^2 x_{NG} \phi_y q_T + \nu_y z_{NG} \phi_y + \phi_y)] \quad (D44)$$

$$598 \quad + f_a [1 + \theta_t \nu_y x_{NR} - \theta_t \nu_y q_T + \nu_y z_{NR}] \quad (D45)$$



599 References

- 600 Bielawa, R.: Rotary wing structural dynamics and aeroelasticity, AIAA education series, American Institute of Aeronautics and Astronautics,
601 2006.
- 602 Branlard, E.: Flexible multibody dynamics using joint coordinates and the Rayleigh-Ritz approximation: The general framework behind and
603 beyond Flex, *Wind Energy*, 22, 877–893, <https://doi.org/10.1002/we.2327>, 2019.
- 604 Branlard, E.: WELIB, Wind Energy Library, GitHub repository <http://github.com/ebranlard/welib/>, 2021.
- 605 Branlard, E., Giardina, D., and Brown, C. S. D.: Augmented Kalman filter with a reduced mechanical model to estimate tower loads on
606 a land-based wind turbine: a step towards digital-twin simulations, *Wind Energy Science*, 5, 1155–1167, [https://doi.org/10.5194/wes-5-](https://doi.org/10.5194/wes-5-1155-2020)
607 1155-2020, 2020a.
- 608 Branlard, E., Jonkman, J., Dana, S., and Doubrawa, P.: A digital twin based on OpenFAST linearizations for real-time load and fatigue esti-
609 mation of land-based turbines, *Journal of Physics: Conference Series*, 1618, 022 030, <https://doi.org/10.1088/1742-6596/1618/2/022030>,
610 2020b.
- 611 Docquier, N., Poncelet, A., and Fisette, P.: ROBOTRAN: a powerful symbolic generator of multibody models, *Mech. Sci.*, 4, 199–219,
612 <https://doi.org/10.5194/ms-4-199-2013>, 2013.
- 613 Gede, G., Peterson, D., Nanjangud, A., Moore, J., and Hubbard, M.: Constrained Multibody Dynamics With Python: From Symbolic Equa-
614 tion Generation to Publication., in: *Proceedings of the ASME 2013 International Design Engineering Technical Conferences and Com-*
615 *puters and Information in Engineering Conference*. Portland, Oregon, USA. August 4-7, <https://doi.org/10.1115/DETC2013-13470>, 2013.
- 616 Geisler, J.: CADynTurb: Wind Turbine Model from OpenFAST Data using CADyn Equations of Motion, [https://github.com/jgeisler0303/](https://github.com/jgeisler0303/CADynTurb)
617 CADynTurb, 2021.
- 618 Jonkman, J., Butterfield, S., Musial, W., and Scott, G.: Definition of a 5MW Reference Wind Turbine for Offshore System Development,
619 Tech. Rep. NREL/TP-500-38060, National Renewable Energy Laboratory, 2009.
- 620 Jonkman, J. M.: Dynamics of offshore floating wind turbines—model development and verification, *Wind Energy*, 12, 459–492,
621 <https://doi.org/10.1002/we.347>, 2009.
- 622 Kane, T. R. and Wang, C. F.: On the Derivation of Equations of Motion, *Journal of the Society for Industrial and Applied Mathematics*, 13,
623 487–492, <https://doi.org/10.1137/0113030>, 1965.
- 624 Kurtz, T., Eberhard, P., Henninger, C., and Schiehlen, W.: From Neweul to Neweul-M2: symbolical equations of motion for multibody system
625 analysis and synthesis, *Multibody System Dynamics*, 24, 25–41, <https://doi.org/10.1007/s11044-010-9187-x>, 2010.
- 626 Kurz, T. and Eberhard, P.: Symbolic Modeling and Analysis of Elastic Multibody Systems, in: *International Symposium on Coupled Methods*
627 *in Numerical Dynamics Split*, Croatia, September 16-19, 2009.
- 628 Lemmer, F.: Low-order modeling, controller design and optimization of floating offshore wind turbines., Ph.D. thesis, Universit at Stuttgart,
629 2018.
- 630 Merz, K. O.: STAS Aeroelastic 1.0 - Theory Manual., Tech. rep., Trondheim, SINTEF Energi AS., 2018.
- 631 MotionGenesis: MotionGenesis™ Kane Tutorial, Tech. rep., Motion Genesis LLC, www.motiongenesis.com, 2016.
- 632 OpenFAST: Open-source wind turbine simulation tool, available at <http://github.com/OpenFAST/OpenFAST/>, 2021.
- 633 Øye, S.: Fix Dynamisk, aeroelastisk beregning af vindmøllevinger, Report AFM83-08, Fluid Mechanics, DTU, 1983.



- 634 Pöschke, F., Gauterin, E., Kühn, M., Fortmann, J., and Schulte, H.: Load mitigation and power tracking capability for wind turbines us-
635 ing linear matrix inequality-based control design, *Wind Energy*, 23, 1792–1809, <https://doi.org/https://doi.org/10.1002/we.2516>, <https://onlinelibrary.wiley.com/doi/abs/10.1002/we.2516>, 2020.
- 636
- 637 Reckdahl, K. and Mitiguy, P.: Autolev Tutorial, Tech. rep., OnLine Dynamics Inc., Sunnyvale CA, 1996.
- 638 Schwertassek, R. and Wallrapp, O.: *Dynamik flexibler Mehrkörpersysteme*. [in German], Friedr. Vieweg & Sohn, Braunschweig, 1999.
- 639 Shabana, A.: *Dynamics of Multibody Systems*, Cambridge University Press, 2013.
- 640 Simani, S.: Advanced Issues of Wind Turbine Modelling and Control, *Journal of Physics - Conference series*, 659, 2015.
- 641 Sønderby, I. and Hansen, M. H.: Open-loop frequency response analysis of a wind turbine using a high-order linear aeroelastic model, *Wind*
642 *Energy*, 17, 1147–1167, <https://doi.org/10.1002/we.1624>, 2014.
- 643 Sympy: <https://www.sympy.org>.
- 644 Verlinden, O., Kouroussis, G., and Conti, C.: EasyDyn: a framework based on free symbolic and numerical tools for teaching multibody
645 systems, in: *Multibody Dynamics 2005, ECCOMAS Thematic Conference*, 2005.
- 646 Wallrapp, O.: Standard Input Data of Flexible Members in Multibody Systems, in: *Advanced Multibody System Dynamics. Solid Mechanics*
647 *and Its Applications*, edited by Schiehlen, W., vol. 20, pp. 445–450, Springer, Dordrecht, https://doi.org/10.1007/978-94-017-0625-4_33,
648 1993.
- 649 Wallrapp, O.: Standardization of flexible body modeling in multibody system codes, part i: Definition of standard input data., *Journal of*
650 *Structural Mechanics*, 22, 283–304, 1994.
- 651 Wallrapp, O. and Schwertassek, R.: Representation of geometric stiffening in multibody system simulation, *International Journal for Numer-*
652 *ical Methods in Engineering*, 32, 1833–1850, <https://doi.org/10.1002/nme.1620320818>, [10.1002/\(ISSN\)1097-0207](https://doi.org/10.1002/(ISSN)1097-0207), 1991.